Series Elastic Tether Management for Rappelling Rovers

Travis Brown, Alessandro Stefanini, Nikola Georgiev, Jacek Sawoniewicz, Issa Nesnas

***Abstract*— The Axel rappelling rover was designed to enable access to intriguing and important science sites that lie in difficult terrains that are inaccessible to conventional rovers. Extended autonomous rappelling calls for careful control of tether tension, precise management of tether spooling, and some measure of shock tolerance. This paper covers the design and testing of a first-generation tether management system (TMS) for Axel. The system uses a double bull-wheel capstan driven by a low-stiffness series elastic actuator (SEA) to provide tension control and decouple internal spooling tension from external tether tension. The benefit of the series elastic actuator is two-fold. First, it permits closed-loop tether tension control with lower mass and power consumption than a comparable torque motor. Second, it improves the shock/drop tolerance of the rappelling system both while moving and when the system is inactive with the motors locked. Experiments on the new TMS show that this design performs well in keeping nearly constant spooling tension while rejecting large dynamic disturbances at the output. While the SEA is very effective at maintaining a given tension contribution, the additional effects of friction and the unique mechanical properties of the tether result in substantial errors in the measured output tension. Upcoming field trials will be used to evaluate the effectiveness and sufficiency of this system when integrated in Axel.**

I. INTRODUCTION

Many high-value science targets on the Moon, Mars, and other planetary bodies have been found in steep terrains that are far beyond the reach of traditional rovers. Such terrains are often on crater walls or on escarpments that are too steep and risky to access or explore [1], [2]. This has motivated the development of the Axel rappelling rover (Fig. 1) which is capable of navigating highly irregular terrains ranging from flat plains to vertical cliffs [3]. The Axel rover descends steep hills or sheer drops by paying out a high-strength rappelling tether from a central spool inside its body. Several field tests [4] have shown the capabilities of this system for accessing hostile terrain [4]. This practical experience has also demonstrated the need for a suite of tether management capabilities to improve reliability in autonomous operation. First, the tether should be controllable to a widely varying levels of tension as demanded by the mobility controller [5]. During an Axel field test, the rover experienced tensions ranging from 0 to 750 N as it rappelled and retracted across a slope ranging from 40 to 80 degree in angle [4]. Second, the tether must be consistently and precisely spooled at a prescribed tension to maximize packing ratio and avoid potentially serious spooling anomalies such as knifing. This is increasingly important over longer distances (200 m - 1 km). Third, the subsystem should be able to absorb shocks to minimize the dynamic loading on the tether in the event of slips and falls in order to minimize the risk of degrading the tether's mechanical and electrical integrity. Since the tether houses relatively stiff power and signal lines, its ability absorb these shocks is limited, motivating this third requirement.

Fig. 1: The Axel rappelling rover descends extreme terrain using a high-strength tether to support its weight and carry power and data.

Closed loop tension control was a design objective for the current Axel, with a series-elastic tension measurement device included in the current spool design [6]. Other work in rappelling robots has similarly identified closed-loop tether tension control as a major enabler of autonomous operation. The TReX rappelling rover incorporated a load-cell sensing system to autonomously pay out or retract tether as needed [7]. In addition to providing tension sensing, the series elastic element in the Axel spool provides some measure of shock tolerance, partially satisfying the third objective. Nevertheless, the current design has no means of isolating spool tension from external tension, making it impossible to simultaneously satisfy all three objectives. This has motivated the development of a tether management system (TMS) that enables level winding, external tension control, shock tolerance, and independent spooling tension control.

II. TETHER MANAGEMENT SYSTEM DESIGN

The general architecture of the new Tether Management System (TMS) is shown in Figure 2. It generally consists of

This research was carried out at the Jet Propulsion Laboratory, California Institute of Technology, under a contract with the National Aeronautics and Space Administration.

Travis Brown, Alessandro Stefanini, Jacek Sawoniewicz, and Issa Nesnas are with the Jet Propulsion Laboratory, California Institute of Technology, 4800 Oak Grove Dr., Pasadena, CA, 91109 travis.l.brown@jpl.nasa.gov

Nikola Georgiev, Department of Mechanical Engineering, California Institute of Technology georgiev@caltech.edu

two stages: (1) an output stage that is responsible for generating the large, external tension commanded by the mobility system and responding dynamically to exogenous tether movement (2) a spooling system that stores the tether on a precisely wound spool at low tension. The first stage, called the Primary Tension Module (PTM) uses a double bullwheel capstan (or traction winch) to isolate the external mobility tension from the internal spooling tension. The capstan is driven through a series elastic actuator (SEA), providing shock/drop tolerance and tension measurement/control. The second stage consists of an elastic tensioner, called the slack buffer, a level-winding mechanism, and a spool. The slack buffer decouples the motion of the spool from the motion of the capstan and measures spool tension. This prevents the inertia of the spool from being felt at the output. It also allows the spool tension controller to be less aggressive/responsive while still maintaining tension on the spool side of the PTM.

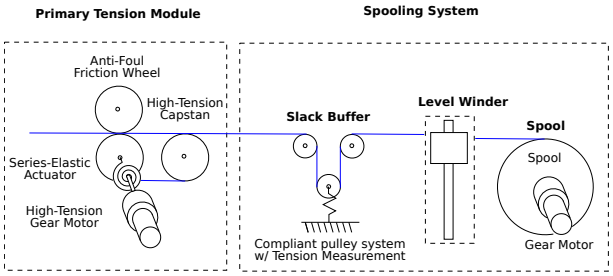

Fig. 2: Tether Management System

Many control schemes have been proposed for series elastic actuators [8], [9]. The system discussed here is particularly interesting due to the potential for coordinated MIMO control between the two elastic systems (PTM and spool). Nevertheless, as a first step, this work assumes that the PTM and spool tension control can be treated as decoupled systems and controlled independently. This requires that the effect of each controller on the other is negligible and can be can be treated a disturbance. This is generally a valid approach if the magnitude of the interaction is small or the systems operate at significantly different frequencies. A simulation model was created to examine these effects and inform the mechanical design. Individual PID controllers were designed for each subsystem and the resulting model was used to simulate several worst case scenarios. Interaction between the two systems was found to be minimal as long as the slack buffer spring was sufficiently soft and had sufficient travel to absorb transients from the PTM without bottoming out.

A. Primary Tension Module (PTM)

The PTM uses an SEA to provide the tension control and drop tolerance needed for Axel. SEAs have been a significant focus in robotics research since the mid 1990's. They exhibit lower output impedance and more precise force control compared to stiff actuators, and improved weight and efficiency compared to direct drive torque motors [10]. The primary challenges in SEAs are increased control complexity and limited bandwidth.

Recent work with SEAs has generally tended to use stiffer springs to provide higher bandwidth and more accurate dynamic force control [11]. This requires a high performance control system and leads to increased motor-locked output impedance. This is not the approach taken in this work. This work targets space applications where electrical and computational power are limited, making high performance controllers less attractive. Motors are frequently locked and disabled whenever possible, calling for an approach that does not rely on active control to yield low output impedance. Moreover, rovers tend to move slowly, reducing the need for a high performance system.

Specification of the PTM spring stiffness requires balancing two competing objectives. It is well known that the bandwidth of a series elastic actuator is proportional to the stiffness of the spring [12][10]. On the other hand, the SEA must be as soft as possible to absorb shock loading and protect the tether in case of falls. As is the case with climbing ropes, the tether itself is compliant and provides some level of drop tolerances proportional to the amount of tether over which the drop is be absorbed. This leads to the concept of fall-factor, which is the ratio of the fall height to the tether length.

$$\mathbb{F} = \frac{h}{l_{tether}} \tag{1}$$

More compliant tethers with higher breaking strength are capable of handling larger fall factors. The allowable fall factor is given by

$$\mathbb{F}_{max} = \frac{T_{max}^2}{2gmEA}, \tag{2}$$

where g is gravity, m is inertia that must be accelerated/decelerated, T_{max} is the tension limit of the tether, E is Young's modulus, and A is the cross sectional area. Axel currently has a mass of 54 kg and uses a tether with an axial rigidity $EA = 44500$ N/% and a maximum tension of 4454 N. Assuming the tether is rigidly attached to Axel, the maximum fall factor would be 0.42. The literature on the dynamic behavior of ropes, however, indicates that they exhibit viscoelasticity, leading to a dynamic stiffness typically three times the static stiffness of the rope [13]. Using this multiplier, the maximum fall factor for Axel is 0.143.

The PTM places a spring in series with the tether, directly increasing the maximum fall factor. Moreover, if the motor brake is released, the only inertia that must be accelerated passively is the motor drivetrain rather than the whole robot. The full inertia of the robot can then be slowed actively by the PTM motor at a controlled rate. Since the spring stiffness is fixed, as the free tether length increases, the overall stiffness will eventually converge to that of the tether. Fortunately, Axel's tether periodically forms new anchor points via contact with the terrain, limiting the range of free tether. In this work it is assumed that 10 m is the maximum tether length between anchor points. Competing

with the need for a soft spring is the desire for high tension control bandwidth. While many factors affect SEA bandwidth, some guidelines exist to estimate general performance limits. Using motor specifications, and reasonable guesses for bearing and gearbox friction, the large-force bandwidth can be estimated using the approach shown in [12]. This treats the back-emf of the motor as damping force and computes a combined damping ratio for the motor/spring system. The PTM motor and gear ratio were chosen to meet the static load requirements of the PTM, while providing low reflected inertia, mass, and static power consumption. A spring stiffness of 100 Nm/rad was chosen to balance drop tolerance and bandwidth. Figure 3 shows the effective series stiffness and the maximum fall factor for this stiffness over a range of free tether lengths.

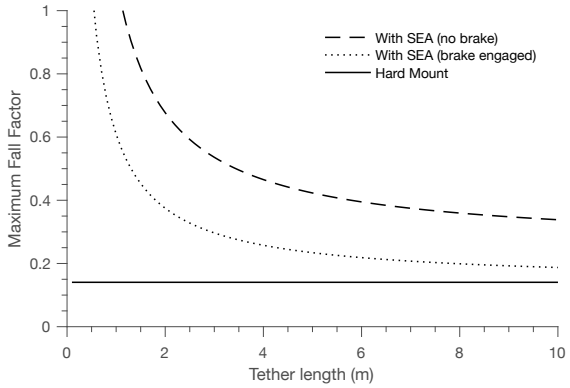

(a) Fall factor comparison.

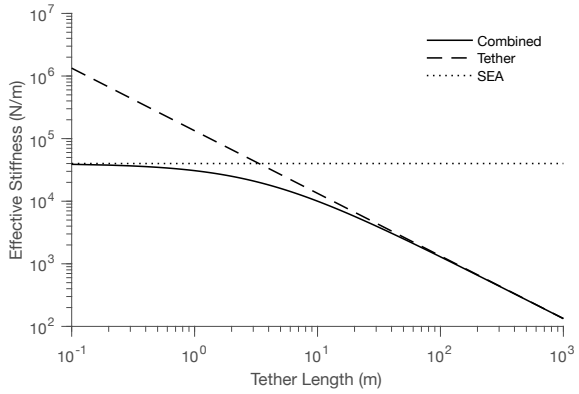

(b) Linear series stiffness with SEA.

Fig. 3: The effect of adding series compliance to the tether management system. Stiffness is reduced and the maximum admissable fall factor improves significantly for shorter tether lengths.

The goal here was to keep the SEA stiffness low enough to provide a measurable benefit over the expected free tether length range of 10 m. This design places the stiffness crossover point at approximately 3.35 m, resulting in the largest benefit at smaller lengths $<$ 5m but still maintaining a significant advantage at 10 m. With this selection, the natural frequency of the motor-gearbox-spring combination is 25 Hz, which combined with the electrical parameters for the motor yields an estimated large-force bandwidth of 3.5 Hz. Typically the achievable controlled bandwidth is 1-5 times the large-force bandwidth [12], [14], suggesting a final achievable bandwidth of 3-15 Hz. While this was deemed sufficient for a slow-moving rover such as Axel, future field testing will be needed to provide verification.

B. Spooling System

The spooling system consists of the slack buffer, the level winder, and the spool. The current Axel spool was reused, but with a re-geared motor to allow faster spooling. This ensures that it can maintain spooling tension even when the PTM is reeling at maximum rate. Previous experiments at JPL had manually tested spooling tension from 0-50N and had shown that higher tension generally led to more reliable spooling, with diminishing returns from 20 N-50 N. Consequently, 50 N was used as the target number for the spooling system, with values as low as 20 N permissible. The new spool motor was designed to continuously deliver 107 N (2x factor of safety) and pay-in at a maximum rate of 0.52 m/s.

The level winder consists of a carriage, riding on a linear slide bearing, and driven by a lead-screw (Fig. 4). Unlike most level windings systems, the lead screw is driven by an independent motor. This allows some flexibility in controlling spooling and avoids the difficulty of transmitting power between the Axel body and the boom to which the level winder is attached. The level winder is designed to handle side loads of up to 500 N (10x factor of safety) while still providing adequate speed to match the spool.

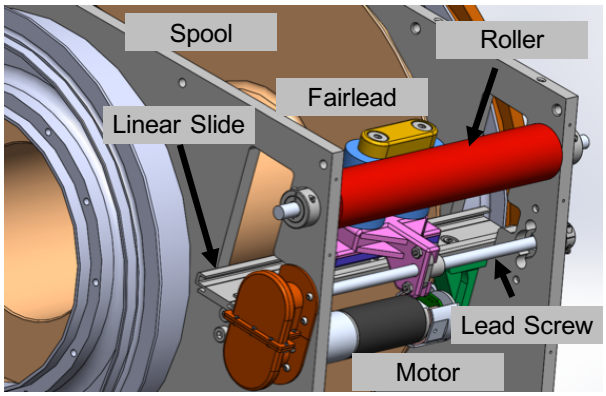

Fig. 4: Level winder for the Axel TMS

The slack buffer consists of a pulley riding on a linear slide bearing. The pulley is anchored on one end with a spring and instrumented with a linear encoder. This linear encoder allows the spool controller to estimate the spooling tension and adjust it as needed. As with the PTM, selecting the spring stiffness is a balance between competing objectives. Softer springs provide greater travel and better decoupling between the PTM and the spooling system, giving the spool more time to react and limiting changes in tension. Stiffer springs provide more reactive behavior, minimizing the chance of a zero tension condition on the input to the PTM (baring buffer saturation). Since the capstan is a friction-based tension

multiplication device, it requires at least some tension on the spool side to apply tension on the output. In simulation, a spring with a stiffness of 400 N/m and 30 cm of travel was found to provide sufficient buffering and minimal loss of tension even with a very slow spool controller. Due to limited selection and packaging constraints, the final as-built system used a stiffer spring (860 N/m) with 9 cm of travel and 9 N preload, leading to a maximum tension of 43 N. The nominal spooling tension was set at 33 N to allow wide movement in either direction before violating tension limits.

III. PTM Physical Design

This section describes the design of the PTM, which consists of a pair of grooved capstans driven by a torsion spring, planetary differential gearbox and a brushless DC motor. Due to the relatively high minimum bend radius (50 mm) given by the manufacturer of the current Axel tether, the capstans were required to be at least 100 mm in diameter. This large size led to a design strategy of packaging the SEA spring inside the capstan in an attempt to save volume (Fig. 5).

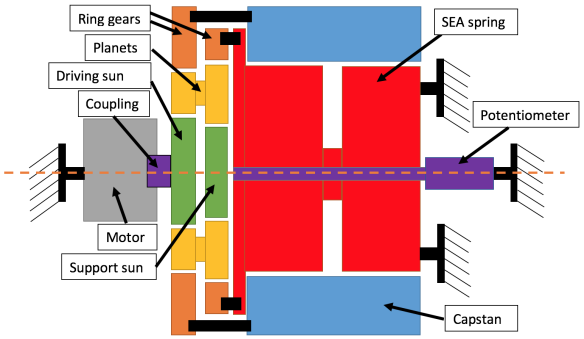

Fig. 5: SEA schematic structure.

A. Spring Design

The SEA spring is a direct application of the design approach described in [15]. The spring target stiffness is 100 Nm/rad with maximum load of 50 Nm, which results in maximum desired displacement of 28.6°. As mentioned, the spring was designed to fit inside the capstan. This compactness requirement motivated a novel spring design. The spring consists of two planar rotary springs that share the same solid cylindrical core and are connected in series. Each of the two series springs has twice the desired SEA stiffness, resulting in the correct stiffness overall. Throughout the design of the spring prototype of [15], the size of the central mounting holes and their radial positions were identified as a major design constraint driving the spring radial size. The dual spring design avoids these issues by placing the mounting holes far from the central axis, leading to a more compact design. The geometry of the design is enabled by metal 3D printing technology. Titanium was chosen because it is readily available and provides excellent strength and weight properties. Figure 6 shows the 3D printed titanium prototype and its a cross-sectional view.

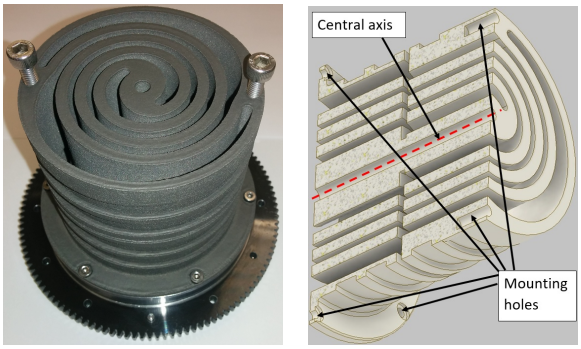

Fig. 6: SEA spring prototype on the left and cross-sectional view on the right.

The SEA prototype is designed for maximum admissible stress at maximum displacement, given by the Ti-6Al-4V fatigue strength of 510 MPa. Finite Element Analysis confirmed the design mechanical properties with an error of $\leq 1\%$ on both the stiffness and the stress values.

B. Gearbox Design

The SEA gearboxes is based on the bearingless planetary gearbox design introduced in [16] and is shown in Figure 7. The gearbox has a 35:1 ratio from motor to capstan and

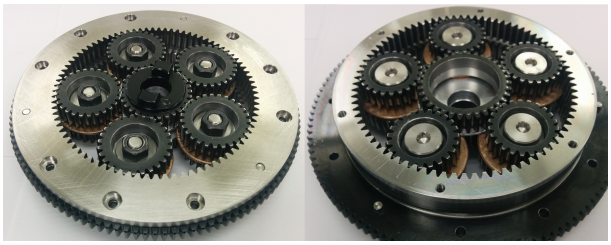

Fig. 7: SEA gearbox prototype.

a 36:1 ratio from motor to spring. It consists of a driving sun gear, a support sun gear, compound planets, stationary ring gear and an output ring gear as shown in Figure 5. Commercial SDP-SI gears were milled out to adapt them to the design. Figure 8 shows a section view of the planet design. A belleville washer provides compression force ensuring a constant frictional coupling between the two gears. The planet is axially constrained by a thrust bearing. A three-piece flexible coupling connects the motor rotor to the driving sun gear as shown in Figure 5.

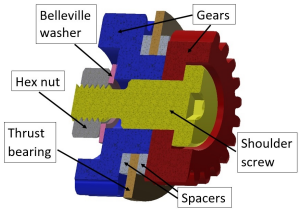

Fig. 8: Compound planet design.

Despite the large commercial gears' normal backlash of around 0.1*mm*, the gearbox is backlash-free. This is achieved by assembling the gearbox utilizing a fixture that constrains the sun and ring gears. The backlash is removed by displacing the gears in each planet with respect to each other before tightening the nut and flattening the belleville washer. Thus, a major advantage of this bearingless planetary gearbox variant is that it can be constructed backlash-free with standard gearing components. The planets mass is,

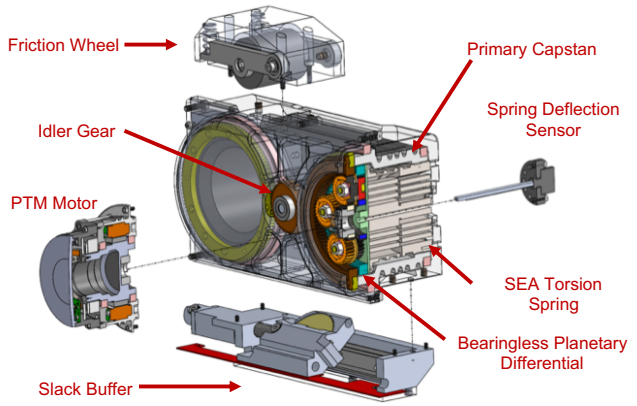

Fig. 9: Exploded view of the PTM showing major components and their layout.

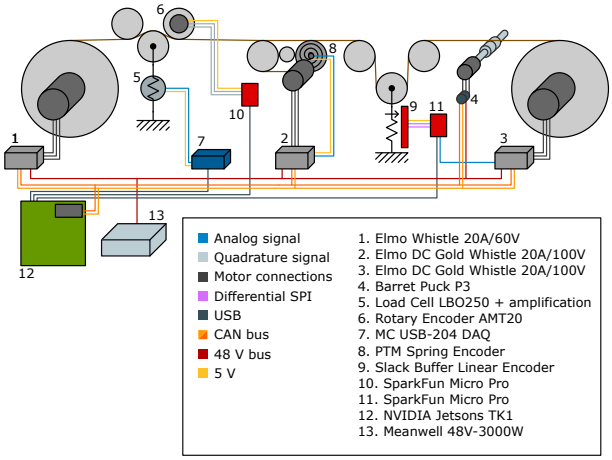

Fig. 10: Test bench system diagram.

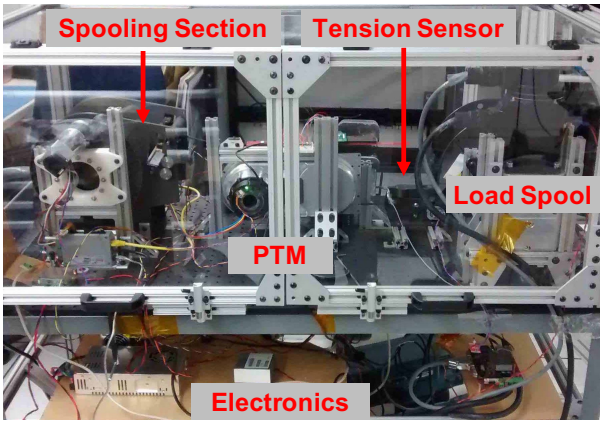

Fig. 11: TMS test bench provides an environment for testing and profiling the behavior of the TMS.

however, significantly higher compared to the thin section design of [16] due to the weight of the screw and hex nut.

The fully customizable bearingless planetary gearbox structure is attractive for SEA applications due to its differential nature. This property is exploited in the SEA design of Figure 5, where none of the ring gears are stationary. One of the ring gears is attached to the capstan and the other ring is coupled to the spring. The sun gear (driven by the motor) controls their relative displacement. The simplified structure allows for direct measurement of the spring displacement because one of the its ends is stationary as shown in Figure 5.

C. Other Design Elements

The PTM uses four thin section bearings to support the two large capstans in the PTM housing. The SEA drives the primary capstan, which in turn drives the secondary capstan through an idler gear (Fig. 9). A spring loaded polyurethane roller presses against the secondary capstan and provides line tension in cases where the PTM is pushing the tether outward. The SEA is driven by a large gap radius RoboDrive ILM85x13, which was chosen for its high torque/inertia ratio. Spring displacement is measured with a high accuracy 120° optical potentiometer (Copal JT22-120) mounted in the outer housing. The total mass of the PTM is approximately 6kg or 10% of the total rover mass as currently constructed.

IV. BENCHTOP TEST SYSTEM

Validation of the TMS was conducted on a purpose-built benchtop test rig (Figure 11). It is composed of three subsystems: the prototype TMS, an industrial motor to simulate loads on the tether and a sensor assembly to measure PTM output performance. All the parts are mounted on a base plate with a grid of threaded holes, allowing to execute multiple types of experiments where the components are differently arranged. For example, a box containing sand can be put between the load motor and the TMS to evaluate the degradation of the tether due to dust collected in the curls.

A. Load motor

The load motor is a Trust Automation SE650-1000 with a Neugart WPLE120 7:1 gearbox, driven by an Elmo Whistle controller (rated $20A/60V$) on a $48V$ bus. Although the SE650 is rated for a much higher armature voltage, around 165 V, it naturally runs at a lower speed when on 48 V, and requires a reduction of 7:1 to produce about 1 m/s on the tether in intermittent operation. With a small ratio gearbox, the reflected inertia is small, allowing a more precise control of the load motor. The load spool acts as a variable ratio reduction as tether is wound and the effective radius changes. The resulting maximum tension and speed capabilities are shown in Table I.

B. Instrumentation

In order to validate the TMS, the tension and position of the tether must be measured at the output of the PTM.

Mode	**Empty spool** (4 cm)	**Full spool** (8cm)
Continuous mode	600 N, 0.5 m/s	300 N, 1 m/s
Intermittent mode	1800 N, 0.45 m/s	950 N, 0.9 m/s

TABLE I: Load spool capabilities.

For this reason, the test bench contains a load cell to determine the tension and a rotary encoder for the position. The load cell is a LBO250 from Transducer Techniques and it measures the force produced by the tether on an idler pulley support. The load cell is interfaced to the main computer through an amplification stage and a 12-bits DAQ (Measurement Computing USB-204). The rotary encoder is connected to a microcontroller that stores the ticks count and provides it to the main computer over USB. The resolution is 0.31*mm* and the maximum speed, limited by the interrupt frequency of the microcontroller, is 30 m/s.

C. Communication, control and software

The main software runs on a NVIDIA TK1 equipped with Ubuntu Linux 14.04, which communicates with all the actuators through CAN bus, as in the actual rover. Responsibilities of the central computer are to start the TMS, drive the load motor and log all the necessary data. Fast logging is required to analyze the performance of the system. This is limited by the CAN bus bandwidth, together with the Elmo communication protocol SimplIQ, which has an average roundtrip time of 1 ms, on average. The software is built on top of CLARAty framework, developed in-house at JPL and introduced in [17].

V. RESULTS

Once the system was constructed and all analog sensors were calibrated, the load spool was locked and the controller gains for the PTM were tuned heuristically to maximize performance (minimum settling time) without compromising stability. The bandwidth of the user-space control loop running on the Elmo was found to be slightly more than 100 Hz (much slower than the anticipated 1 kHz), limiting the overall bandwidth of the torque control loop.

A. Fixed-Output Tests

For tuning purposes, the PTM was commanded to execute a step change from 0 N to 500 N of tension. This corresponds to full Axel weight in earth gravity (for which this system was designed). Gains were limited by high frequency noise in the spring feedback signal. Future work on this system will introduce a low-pass prefilter between the sensor and the motor controller.

The step response showed a settling time of around 0.2 seconds, corresponding to a positioning bandwidth of 5 Hz (consistent with earlier estimates). A sine sweep was then used to directly measure the bandwidth (Figure 13). These results showed a resonant peak and phase reversal at 7 Hz. The PTM was able to faithfully track references up to around 5 Hz. Comparison with the external load cell, however, revealed an unexplained discrepancy. While the PTM spring is faithfully tracking the desired cyclic tension profile, the actual tension seen at the output does go through the same magnitude of variation (Figure 14). It's not immediately clear what is leading to this effect, but the authors believe that it may be related to previously undocumented mechanical

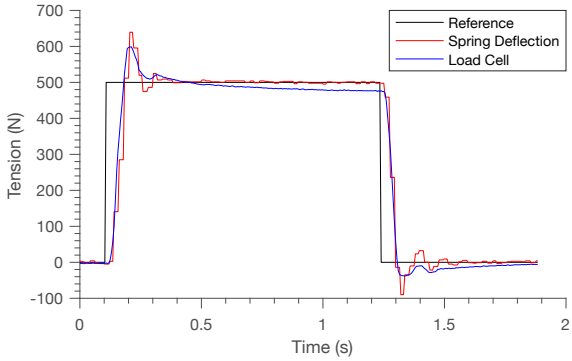

Fig. 12: Step response at full Axel weight. External load cell used to validate tension sensing from spring deflection.

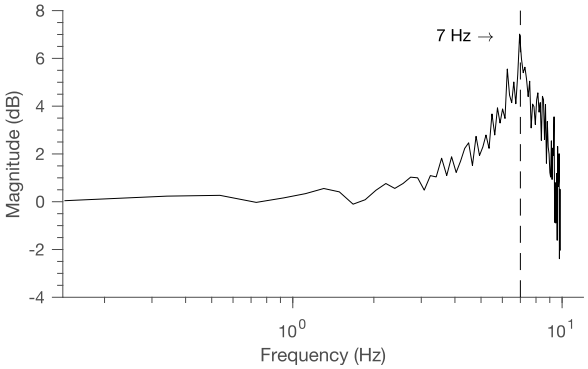

Fig. 13: Bode plot from experimental frequency sweep. System is usable up to 5 Hz, with a resonant peak at 7 Hz.

property of the tether. Specifically, the tether exhibits pronounced "strain stiffening". The tether is typically similar to rope in flexibility, but when exposed to high stress, it becomes semi-rigid until it is flexed under low tension. This may be due to the unique construction of the tether (Fig. 15), which includes woven layers of high-strength material surrounding a central helix of copper conductors. As the tether is stretched, the woven layers tighten around the copper, resulting in high bending resistance. Alternatively, this may come purely from plastic deformation of the copper wires. It is theorized that these effects could lead to large levels of "rolling-resistance" in the capstan when under high tension or potentially alter the forces applied by the tether on the load cell pulley.

B. Shock Loading Test

A major goal of this work is to improve the drop tolerance of Axel under small incidental falls. Several drop simulations were performed with the testbench at its maximum load velocity of 0.5 m/s, with a free tether length ranging from 50cm to 30m. Slack tether was placed between the load spool and the PTM, and both the TMS controller and the load spool were activated. The plot from the 50cm test is shown in Figure 16. Since there is no tension on the tether, the PTM start reeling at maximum rate to increase the tension. This is followed by a point where the tether becomes taut, simulating the drop. The PTM then synchronizes with the load spool

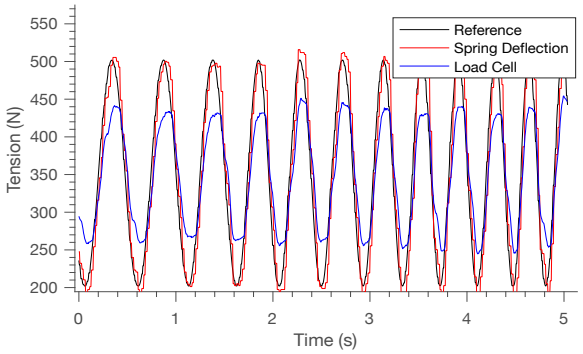

Fig. 14: Comparison of PTM-measured tension and external load-cell tension under cyclic loading. Discrepancy is thought to be due to the unusual strain-stiffening property of the Axel tether.

Fig. 15: The construction of the Axel tether leads to a pronouced strain-stiffening effect. When the tether is pulled taught, it becomes semi-rigid.

and enforces the desired tension value. Meanwhile, the spool tension controller is able to maintain almost perfect tension both before and after the fall.

More extensive tests are needed to test the performance of the system under higher drop velocities not currently possible on the testbench.

C. Disturbance Response Tests

In addition to shock loading, the system was tested for lower frequency disturbance response behavior. A sinusoidal disturbance profile was applied by the load motor while the PTM was commanded to maintain a desired reference tension (Figure 17). Under these conditions, the PTM was able to regulate the tension to within ± 50 N up to 1 Hz and ± 120 N of the reference value over the full frequency range (0.1 to 2 Hz). Once again, a large discrepancy was observed between the PTM-estimated tension and the external measured tension. This was consistent across the full frequency spectrum.

VI. CONCLUSIONS

This paper described the construction and preliminary results of a prototype first generation tether management system for the Axel rover. Using a series-elastic actuator, the system is able to achieve nearly triple the drop tolerance (measured by admissible fall factor) of a stiff system while still delivering a tension control bandwidth of 5Hz

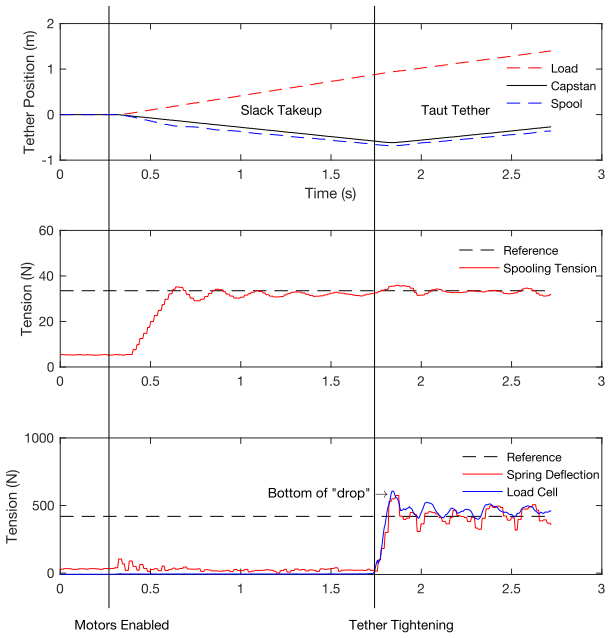

Fig. 16: Performance of the TMS under a simulated drop. Proper spooling tension is maintained throughout the fall and the output tension is controlled to be close to the desired reference. The offset between the spool and capstan due to the tether stored in the slack buffer.

under fixed loading and acceptable tension control under disturbance up to 1 Hz. It is currently unclear what level of performance would be sufficient to satisfy the mobility needs of the rover. Further refinement of the controller, including better filtering and a higher control frequency would substantially improve performance, if necessary.

Tether bend radius restrictions drove the current TMS to be much larger and heavier than necessary. Further investigation of these limits have revealed that they may be overly conservative. The authors plan to design a second generation TMS to fit more compactly into the current rover by exploiting these reduced sizing limits.

The most significant unanswered questions pertain to the previously undocumented strain-stiffening property of the Axel tether, which had a detrimental impact on the measured output tension. This property was not considered in the design of the TMS and may place a limit on the tension control fidelity achievable by such a system. As with the control bandwidth, it's unclear what effect this will have on the overall performance of the system when integrated into Axel. Work is already underway to integrate the TMS into Axel and perform real-world drive testing. The authors anticipate that this testing will be very valuable in both evaluating the current design and informing future TMS refinement and redesign.

VII. ACKNOWLEDGEMENTS

The authors would like to thank and acknowledge the following: NASA Marshal Space Flight Center for lending

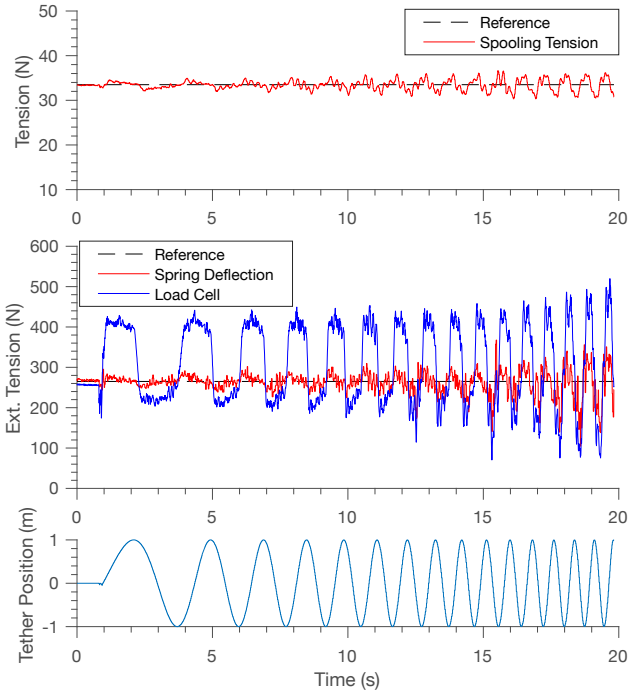

Fig. 17: Behavior of the TMS under a cyclic 1 meter external position disturbance. Spooling tension is almost entirely isolated from the effects. External tension as measured by the SEA is well controlled, but the load cell again indicates a strong friction-like effect from the tether.

their time and manufacturing expertise to support this project, Andre Pate for providing manufacturing consultation, and Evan Yu for design and fabrication work that significantly contributed to the success of this project.

References

[1] L. Kerber, I. Nesnas, L. Keszthelyi, J. W. Head, B. Denevi, P. O. Hayne, K. Mitchel, J. Ashley, J. Whitten, A. Stickle, M. Paton, K. Donaldson-Hanna, R. Anderson, D. Needham, P. Isaacson, and L. Jozwiak, "Moon diver: A discovery mission concept for understanding the history of the mare basalts through the exploration of a lunar mare pit," in *49th Lunar and Planetary Science Conference*, 2018.

[2] G. Meirion-Griffith, I. Nesnas, L. Kerber, R. Anderson, T. Brown, F. Calef, J. Burdick, and M. Tanner, "Accessing mars recurring slope lineae: Mobility systems analysis," in *2018 IEEE Aerospace Conference*, March 2018.

[3] I. A. D. Nesnas, P. Abad-Manterola, J. A. Edlund, and J. W. Burdick, "Axel mobility platform for steep terrain excursions and sampling on planetary surfaces," in *2008 IEEE Aerospace Conference*, March 2008, pp. 1–11.

[4] I. A. Nesnas, J. B. Matthews, P. Abad-Manterola, J. W. Burdick, J. A. Edlund, J. C. Morrison, R. D. Peters, M. M. Tanner, R. N. Miyake, B. S. Solish, and R. C. Anderson, "Axel and duaxel rovers for the sustainable exploration of extreme terrains," *Journal of Field Robotics*, vol. 29, no. 4, pp. 663–685, 2012. [Online]. Available: http://dx.doi.org/10.1002/rob.21407

[5] E. Ferrentino, "Tethered mobility and control for extreme terrain rovers," Master's thesis, Polytechnic University of Turin, 2014.

[6] J. B. Matthews and I. A. Nesnas, "On the design of the axel and duaxel rovers for extreme terrain exploration," in *2012 IEEE Aerospace Conference*, March 2012, pp. 1–10.

[7] P. McGarey, M. Polzin, and T. D. Barfoot, "Falling in line: Visual route following on extreme terrain for a tethered mobile robot," in *2017 IEEE International Conference on Robotics and Automation (ICRA)*, May 2017, pp. 2027–2034.

[8] N. Paine, S. Oh, and L. Sentis, "Design and control considerations for high-performance series elastic actuators," *IEEE/ASME Transactions on Mechatronics*, vol. 19, no. 3, pp. 1080–1091, June 2014.

[9] S. Yoo and W. K. Chung, "Sea force/torque servo control with model-based robust motion control and link-side motion feedback," in *2015 IEEE International Conference on Robotics and Automation (ICRA)*, May 2015, pp. 1042–1048.

[10] G. Pratt and M. Williamson, "Series elastic actuators," in *Intelligent Robots and Systems 95. 'Human Robot Interaction and Cooperative Robots', Proceedings. 1995 IEEE/RSJ Int. Conference on*, vol. 1, Aug 1995, pp. 399–406 vol.1.

[11] N. Paine, J. S. Mehling, J. Holley, N. A. Radford, G. Johnson, C.-L. Fok, and L. Sentis, "Actuator control for the nasa-jsc valkyrie humanoid robot: A decoupled dynamics approach for torque control of series elastic robots," *Journal of Field Robotics*, vol. 32, no. 3, pp. 378–396, 2015. [Online]. Available: http://dx.doi.org/10.1002/rob.21556

[12] D. Robinson, J. Pratt, D. Paluska, and G. Pratt, "Series elastic actuator development for a biomimetic walking robot," in *Advanced Intelligent Mechatronics, 1999. Proceedings. 1999 IEEE/ASME Int. Conference on*, 1999, pp. 561–568.

[13] K. Bitting, "The dynamic behavior of nylon and polyester line," *U.S. Coast Guard Research and Development Center Final Report*, 1980.

[14] J. W. Sensinger and R. F. Weir, "Design and analysis of a non-backdrivable series elastic actuator," in *9th International Conference on Rehabilitation Robotics, 2005. ICORR 2005.*, June 2005, pp. 390–393.

[15] N. Georgiev and J. Burdick, "Design and analysis of planar rotary springs," in *2017 IEEE/RSJ International Conference on Intelligent Robots and Systems (IROS)*, Sept 2017, pp. 4777–4784.

[16] ——, "Design and analysis of the bearingless planetary gearbox," in *2017 IEEE/RSJ International Conference on Intelligent Robots and Systems (IROS)*, Sept 2017, pp. 1987–1994.

[17] R. Volpe, I. Nesnas, T. Estlin, D. Mutz, R. Petras, and H. Das, "The claraty architecture for robotic autonomy," in *2001 IEEE Aerospace Conference Proceedings (Cat. No.01TH8542)*, vol. 1, 2001, pp. 1/121–1/132 vol.1.